Physics and Imaging in Radiation Oncology 21 (2022) 54–61

Contents lists available at ScienceDirect

Physics and Imaging in Radiation Oncology

journal homepage: www.sciencedirect.com/journal/physics-and-imaging-in-radiation-oncology

Original Research Article

Inter- and intrafraction motion assessment and accumulated dose quantification of upper gastrointestinal organs during magnetic resonance-guided ablative radiation therapy of pancreas patients

Sadegh Alam [a], Harini Veeraraghavan [a], Kathryn Tringale [b], Emmanuel Amoateng [b], Ergys Subashi [a], Abraham J. Wu [b], Christopher H. Crane [b], Neelam Tyagi [a,*]

[a] Department of Medical Physics, Memorial Sloan-Kettering Cancer Center, New York, NY 10065, USA
[b] Department of Radiation Oncology, Memorial Sloan-Kettering Cancer Center, New York, NY 10065, USA

ARTICLE INFO

Keywords:
Deformable image registration (DIR)
LDDMM
1.5 T magnetic field
MR-guided radiation therapy
MR-linac

ABSTRACT

Background and purpose: Stereotactic body radiation therapy (SBRT) of locally advanced pancreatic cancer (LAPC) is challenging due to significant motion of gastrointestinal (GI) organs. The goal of our study was to quantify inter and intrafraction deformations and dose accumulation of upper GI organs in LAPC patients.
Materials and methods: Five LAPC patients undergoing five-fraction magnetic resonance-guided radiation therapy (MRgRT) using abdominal compression and daily online plan adaptation to 50 Gy were analyzed. A pre-treatment, verification, and post-treatment MR imaging (MRI) for each of the five fractions (75 total) were used to calculate intra and interfraction motion. The MRIs were registered using Large Deformation Diffeomorphic Metric Mapping (LDDMM) deformable image registration (DIR) method and total dose delivered to stomach_duodenum, small bowel (SB) and large bowel (LB) were accumulated. Deformations were quantified using gradient magnitude and Jacobian integral of the Deformation Vector Fields (DVF). Registration DVFs were geometrically assessed using Dice and 95th percentile Hausdorff distance (HD95) between the deformed and physician's contours. Accumulated doses were then calculated from the DVFs.
Results: Median Dice and HD95 were: Stomach_duodenum (0.9, 1.0 mm), SB (0.9, 3.6 mm), and LB (0.9, 2.0 mm). Median (max) interfraction deformation for stomach_duodenum, SB and LB was 6.4 (25.8) mm, 7.9 (40.5) mm and 7.6 (35.9) mm. Median intrafraction deformation was 5.5 (22.6) mm, 8.2 (37.8) mm and 7.2 (26.5) mm. Accumulated doses for two patients exceeded institutional constraints for stomach_duodenum, one of whom experienced Grade1 acute and late abdominal toxicity.
Conclusion: LDDMM method indicates feasibility to measure large GI motion and accumulate dose. Further validation on larger cohort will allow quantitative dose accumulation to more reliably optimize online MRgRT.

1. Introduction

Pancreatic cancer is the fourth leading cause of cancer-related death in the US and has the highest mortality rate of all cancers [1]. Surgery still represents the only curative treatment. However, 30–40% of patients present with locally advanced pancreatic cancer (LAPC) and are deemed unresectable [2–4]. Standard radiotherapy approaches, commonly delivering 40 to 60 Gy in 1.8–2.0 Gy per fraction, add minimal to no survival benefit over chemotherapy alone for patients with locally advanced unresectable pancreatic cancer [5–7]. Our group has shown that ablative radiation doses of >100 Gy_{10} biological equivalent dose produces results that are comparable to surgery in patients with inferior prognostic features [8,9]. The ablative dose prescribed to the target is limited by the dose tolerance and tight dose-volume constraints of nearby radiosensitive gastrointestinal (GI) organs such as stomach, duodenum and small bowel surrounding the disease. Exceeding these tolerances could result in normal tissue toxicity such as bleeding, ulceration, and perforation. Treatment delivery of such ablative doses, when given in fewer fractions, is also complicated by the significant inter and intrafractional motion and appearance variability of gastrointestinal (GI) organs. The interfraction variability can be addressed by magnetic resonance guided adaptive radiotherapy (MRgART) systems

* Corresponding author at: Department of Medical Physics, Memorial Sloan-Kettering Cancer Center, 545 East 74th Street, New York, NY 10021, USA.
E-mail address: tyagin@mskcc.org (N. Tyagi).

https://doi.org/10.1016/j.phro.2022.02.007
Received 29 July 2021; Received in revised form 2 February 2022; Accepted 11 February 2022

that have enabled delivery of ablative doses using five fraction stereotactic body radiation therapy (SBRT) treatments to pancreatic tumors by allowing real time adaptation of dose distribution to account for day-to-day variation in luminal organ shapes and position [10–12].

Although day-to-day interfraction motion can be accounted for by daily online adaptation, a lack of objective and reliable methods for estimating the total cumulative dose delivered to the mobile GI organs-at-risk (OARs), including both the spatial and temporal variation of the maximum dose to the OARs, still presents a clinical challenge. Motion and deformation of GI organs during treatment presents an added challenge and motivation to precisely and accurately measure the dose delivered to the GI organs. However, due to lack of reliable and accurate automated methods to objectively quantify the dose delivered to the OARs, in the effort to limit dose, the OARs are over-constrained by adding larger safety margins. This approach limits the achievable target coverage with ablative doses and the number of patients that can be treated to potentially curative doses. Currently available deformable image registration (DIR) methods implemented on clinical commercial MRgRT systems lack accuracy for deformable anatomies such as prostate and head and neck [13,14]. The MR-MR DIR was also not able to account for large volume changes such as those seen in bladder or rectum [13]. The MR-MR DIR in these commercial systems is also insufficiently accurate for aligning highly deforming and irregularly shaped organs such as upper GI OARs as shown in Fig. 1.

In particular, prior literature includes few investigations into DIR methods applied to highly deforming organs such as small and large bowel and the stomach_duodenum as well as methods to compute accumulated doses during and between treatment fractions. Liu et al quantified day-to-day anatomical variation of GI organs on daily CT scans by estimating a center of mass displacement of 6 mm and 10 mm on the duodenum and stomach [15]. More recently, Magallon-Baro et al [16] estimated inter-fraction motion of 10 ± 4 mm, 6 ± 3 mm and 10 ± 3 mm for stomach, duodenum and bowel in their SBRT cohort treated using Cyberknife with integrated CT-on-rails. The group also performed principal component analysis to generate meaningful anatomies to reproduce clinically delivered doses. Eigen modes representing 90% of the variance represented majority of the large deformations (10 mm on the stomach and bowel and 6 mm on the duodenum) of these OARs. This daily interfraction motion translated to over-irradiation of critical structures adjacent to the tumor such as duodenum and stomach and the dosimetric impact was predominant on small volumes of tissues (e.g. Dmax) [17]. Recently, a deep learning-based DIR method for aligning GI OARs from CT-to-CBCT images was published and shows promising results [18]. To our knowledge, no prior studies have reported MR-to-MR deformation for upper GI OARs including stomach and the duodenum, as well as small and large bowel. Therefore, in this study, we have quantified the inter and intrafraction deformations and the accumulated dose for the afore-mentioned upper GI organs from daily high resolution three-dimensional (3D) T2w MRIs for LAPC patients undergoing MR-guided ablative SBRT on 1.5 Tesla MR-linac system using an in-house developed Large Deformation Diffeomorphic Metric Mapping (LDDMM) deformable registration method.

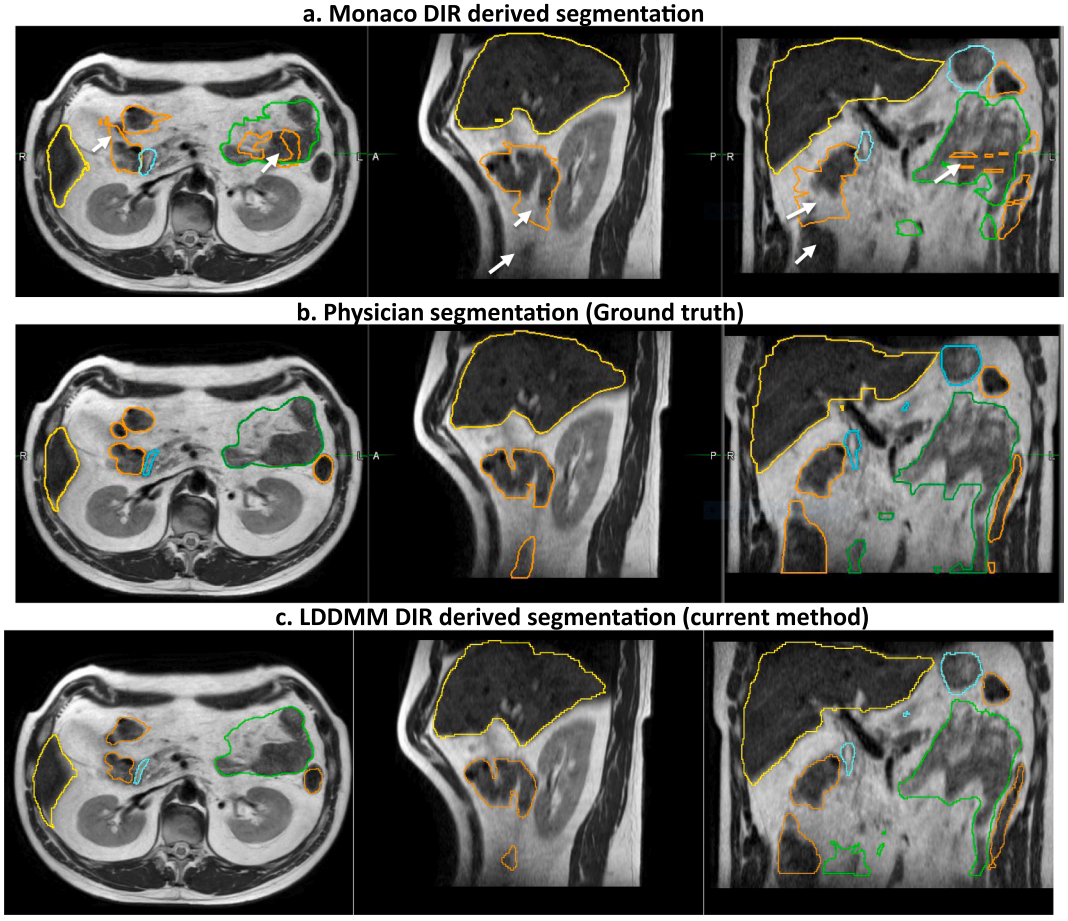

Fig. 1. DIR propagated OAR segmentation produced using a) commercial DIR available in the Monaco treatment planning system for Elekta Unity MR-linac b) Physician ground truth segmentations and c) Large Deformation Diffeomorphic Metric Mapping (LDDMM) method. Segmentations for Liver (Yellow), Large Bowel (light brown), Small Bowel (green) and Stomach_duodenum (cyan) are shown. Poor or no segmentations resulting from commercial DIR method are shown in white arrows. (For interpretation of the references to colour in this figure legend, the reader is referred to the web version of this article.)

2. Materials and methods

2.1. Patient imaging and planning details

On-treatment MRIs from five LAPC patients undergoing five fraction MR-guided SBRT to a total dose of 50 Gy using a pneumatic compression belt were analyzed. The study was conducted under MSKCC IRB approved retrospective protocol number 21–129. The pneumatic pressure level was set in consultation with the patient to minimize gross tumor volume (GTV) and adjacent organ motion within 5 mm. The details of our treatment workflow were recently published [19]. During each treatment fraction, a set of three 3D T2w MRIs (TR/TE = 1300/87 ms, voxel size = 1 × 1 × 2 mm^3, FOV = 400 × 450 × 250 mm^3) – pretreatment, verification and post-treatment were acquired. Verification MRI was acquired immediately before beam-on to confirm patient anatomy has not changed during contouring and adaptive planning. Post-treatment MRI was acquired at the end of treatment. Daily online planning was performed using Elekta's Adapt-to-Shape workflow [20]. A new adaptive plan was generated on the pre-treatment MRI in the Monaco treatment planning system for every fraction using fluence optimization and bulk electron density assignment derived from reference planning CT or prior MR. Interfraction motion was assessed by comparing OAR deformation between the pre-treatment MRI of the first fraction from the remaining four fractions. Intrafraction motion was assessed by comparing OAR deformation between pre-treatment, verification, and post-treatment MRI of each treatment fraction. Three organs were analyzed – stomach_duodenum, small bowel, and large bowel. These three structures were contoured on each of the seventy-five 3D T2w MRI images by an expert medical student (AM) and independently verified by the radiation oncologists (KT, CC). A representative example case with contours for stomach_duodenum, small bowel, and large bowel for all five fractions is shown in Fig. 2. The physician contours were also used as ground truth to assess the accuracy of the DIR algorithm. Each patient was prescribed an ablative dose of 50 Gy in five fractions. The adaptive plan generated on pre-treatment MRI was also copied to verification and post-treatment MRI and doses were recalculated to assess intrafraction dose accumulation. The dose constraints to GI organs were defined as Dmax or D0.035 $cm^3 \leq 33$ Gy and D5$cm^3 \leq$ 25 Gy. D5cm^3 for large bowel was ≤ 30 Gy.

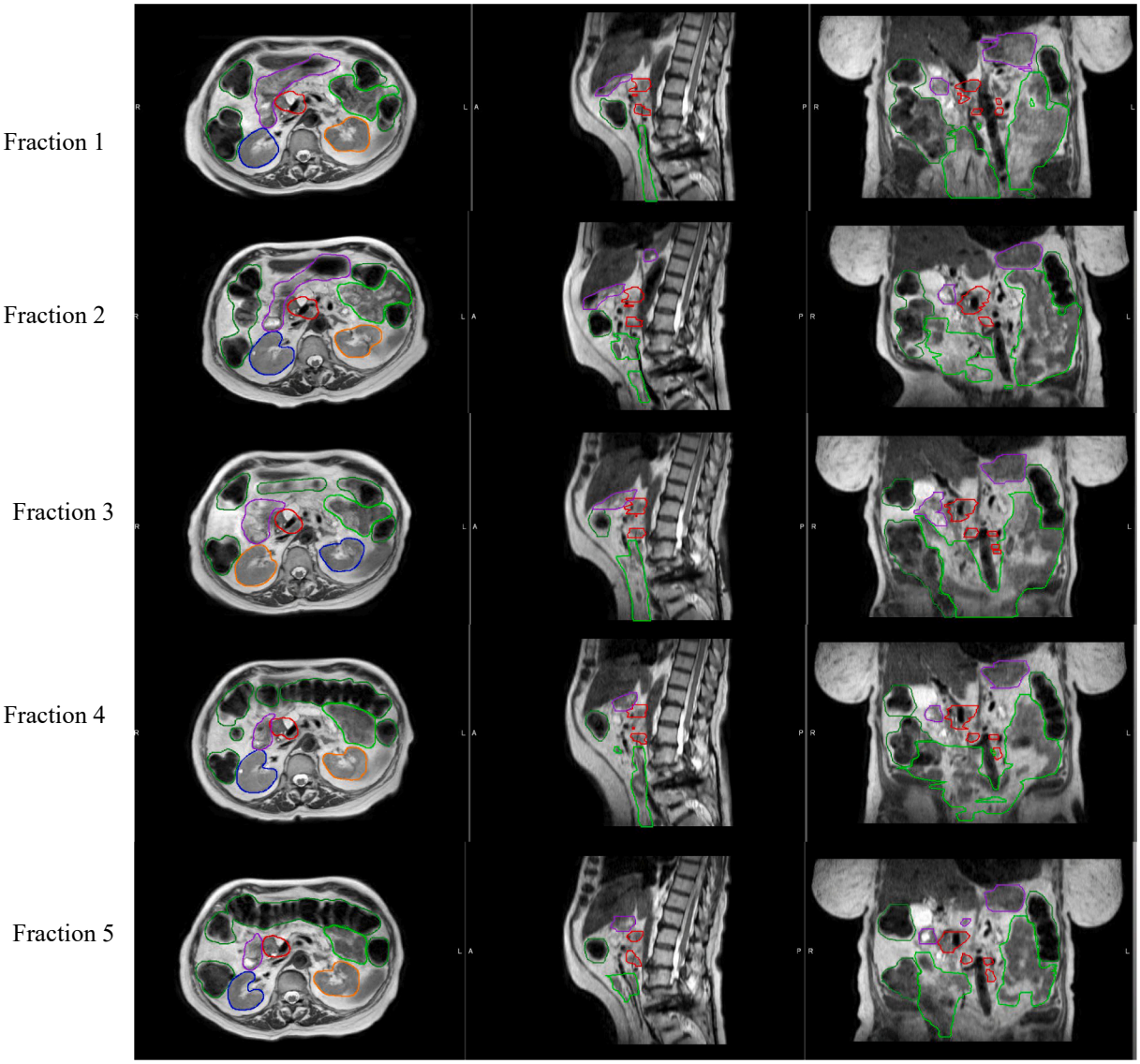

Fig. 2. An example patient case with contours for stomach_duodenum (purple), small bowel (light green) and large bowel (dark green) for all five fractions indicating large inter-fraction motion of GI organs. Other structures include GTV (red) and kidneys (left orange; right blue). (For interpretation of the references to colour in this figure legend, the reader is referred to the web version of this article.)

2.2. Deformable image registration method

The inter-fractional registrations were performed sequentially between a pair of pre-treatment MRI images in consecutive fractions, i.e Fx1 → Fx2, Fx2 → Fx3 and so on. Intrafraction registration for each fraction was performed from verification to pre- and post-treatment to pre-treatment MRI. A multi-stage registration approach was used. The first stage performed a global alignment of the MRIs to spatially align the OARs. This stage used a sequence of rigid and affine image registrations. In the next stage, a DIR was performed using an integrated B-spline regularized method called Symmetrized Large Deformation Diffeomorphic Metric Mapping (LDDMM) registration [21–23] to capture the large organ deformations. The B-spline regularization was performed by fitting a Deformation Vector Field (DVF) to a B-spline object, which gives free-form elasticity to the converging/diverging vectors and represents a morphological shrinkage/expansion. Because the GI organs also exhibit large out-of-plane deformations, we employed a multi-objective registration that minimizes both image intensity differences and geometric change of the contours in the optimization function using Mean Square similarity energy. The geometry objective is enforced using organ delineations, which provide a structure guidance for registration. Equation (1) defines the objective function used for DIR optimization, where $\varphi(x)$ is the transformation between baseline I_b (moving) and follow-up I_f (target) images:

$$C\left(\varphi(x), I_b^{\circ} I_f\right) = w_{image} E^{intensity}_{similarity}(\varphi(x)) + w_{contours} E^{geometry}_{similarity}(\varphi(x)) + Regularizer(\varphi(x)) \quad (1)$$

Consequently, separate cost metrics and their derivatives were computed for the stomach_duodenum, small and large bowel structures along with the images. The metric derivatives were combined at each iteration using scalar weights of 1.0 for small and large bowels, 0.9 (10% less) for stomach_duodenum and 1.2 (20% more) for the images. The weights were obtained experimentally based on significantly larger volumes of the small and large bowels (population mean of 597 cm^3 and 504 cm^3, respectively) compared to stomach_duodenum (242 cm^3). Three levels of multi-resolution registration were used with B-spline mesh size of 16 mm at the coarsest level that was reduced by a factor of two at each sequential level. The optimization step size was set to 0.2 and the number of iterations (100, 70, 30) at each level. Before the registrations, histogram matching [24] was performed to standardize the intensity between the moving and target MRIs.

2.3. Data analysis

Inter and intrafraction deformations and motions within each OAR were quantified for each direction (*i.e.* Left-Right [LR], Anterior-Posterior [AP], Superior-Inferior [SI]) using voxel-wise average and maximum gradient magnitude of the DVF calculated from LDDMM DIR between pre-treatment MRIs and during treatment MRIs of all the fractions. Geometric evaluation of the registrations was assessed using Dice similarity coefficient (DSC) and 95th percentile Hausdorff distance (HD95) calculated between deformed contours and manually drawn ground truth contours for stomach_duodenum, small bowel, and large bowel. DSC and HD95 was also compared between rigid and DIR registrations. Rigid registration was used for comparison as this represents the worst-case scenario. A voxel-wise calculation of Jacobian determinant (J) of the deformations was performed to determine the amount of compression or expansion. J was calculated at each voxel as the determinant of the gradient of the DVF that measured the ratio of local volume change where $J > 1$ indicates local volume expansion, $J < 1$ shrinkage and $J = 1$ no change [23,25]. The Jacobian integral defined as [(Mean J – 1) × structure volume] measured the net local volume change. The correlation between the local volume change of each structure obtained using Jacobian integral and the volume change obtained from the ground-truth contours by the physician was calculated [22,26] by generating scatter plots.

OAR doses for each patient were accumulated using the voxel-by-voxel correspondence built via DIR between each fraction MRI and during treatment MRIs. The deformed dose voxels were summed based on trilinear interpolation that minimized uncertainties and unnecessary discontinuities/distortions in large deformation area in the calculated warped doses [27]. The prescribed dose map in each fraction was scaled to five fractions and for each fraction, the DVF was used to first accumulate intrafraction doses from post-treatment to pretreatment MRI. This was followed by interfraction dose accumulation on the pretreatment MRI from the previous fraction to the current fraction. Accumulated dose-volume parameters such as D0.035 cm^3 and D5cm^3 were extracted for stomach_duodenum, small bowel, and large bowel and compared with our published departmental constraints for 50 Gy in five fractions [19]. To evaluate the dosimetric performance of DIRs, the agreements between the accumulated dose-volume parameters derived from deformed contours and the ground-truth manual contours between each fraction were compared using Bland-Altman plots [28].

3. Results

DSC and HD95 for stomach_duodenum, small bowel, and large bowel were calculated between subsequent fraction deformation for all the patients and compared with rigid registration (supplementary Fig. 1). Median DSC and HD95 for the rigid vs. DIR methods were stomach_duodenum (0.7, 7.9 mm) vs. (0.9, 1.0 mm), small bowel (0.7, 14.6 mm) vs. (0.9, 3.5 mm), and large bowel (0.7, 11.5 mm) vs. (0.9, 2.0 mm).

Inter and intrafraction deformations and motions were calculated from the gradient magnitude of DVFs between pre-treatment MRIs and during treatment MRIs of all the fractions and summarized in Table 1. Intrafraction displacement from pre-treatment to post-treatment as well as pre-treatment to verification MRI were calculated. Median(range) interfraction deformation for stomach_duodenum, small bowel and large bowel were 6.4 (0.0–25.8) mm, 7.9 (0.0–40.5) mm and 7.6 (0.0–35.9) mm. Median intrafraction deformation from pre-treatment to post-treatment MRI were 5.5 (0.0–22.6) mm, 8.2 (0.0–37.8) mm and 7.2 (0.0–26.5) mm. All OARs showed maximum deformation of 2 cm or larger indicating large inter and intrafraction displacement.

The 3D deformation displacement map for stomach_duodenum, small bowel and large bowel was extracted to show the regions of large displacement between Fx1->Fx2 for all five patients (Fig. 3). Our analysis showed that the regions of large displacements varied from patient-to-patient. The boxplots for maximum and average displacement in AP, LR and SI direction for stomach_duodenum, small bowel and large bowel were also calculated (supplementary Fig. 2).

There was a reasonable correlation between the Jacobian integral and volume changes calculated from the ground truth contours for stomach_duodenum, small bowel, and large bowel (see scatter plot supplementary Fig. 3). Percentage difference (mean%±std%) between the volume change calculated by Jacobian integral and physician's ground-truth for stomach_duodenum, large bowel and small bowel were 0.6%±0.6%, 2.9%±10.7% and 3.8%±11.4%. The scatter plot for small bowel indicates large deformations as compared to stomach_duodenum

Table 1
Median (range) inter and intrafraction displacements for stomach_duodenum, small bowel and large bowel.

	Stomach_duodenum		Small Bowel		Large Bowel	
	Median (mm)	Range (mm)	Median (mm)	Range (mm)	Median (mm)	Range (mm)
$Intra_{Pre->post\ (fx1)}$	4.5	[0–20.9]	7.1	[0–36.3]	8.2	[0–41.0]
$Intra_{pre->ver\ (fx1)}$	5.5	[0–22.5]	5.8	[0–40.9]	8.4	[0–38.3]
$Inter_{fx1->fx2}$	6.5	[0–29.0]	10.4	[0–43.2]	11.4	[0–48.0]
$Intra_{Pre->post\ (fx2)}$	5.2	[0–21.5]	8.9	[0–34.9]	7.7	[0–31.2]
$Intra_{pre->ver\ (fx2)}$	4.6	[0–21.7]	6.9	[0–32.3]	7.2	[0–31.3]
$Inter_{fx2->fx3}$	7.7	[0–31.6]	7.8	[0–42.8]	7.7	[0–35.9]
$Intra_{Pre->post\ (fx3)}$	5.9	[0–23.7]	7.6	[0–42.7]	7.4	[0–28.4]
$Intra_{pre->ver\ (fx3)}$	5.0	[0–21.2]	6.3	[0–40.7]	5.8	[0–27.3]
$Inter_{fx3->fx4}$	6.3	[0–22.7]	8.0	[0–36.6]	7.4	[0–35.2]
$Intra_{Pre->post\ (fx4)}$	6.2	[0–26.4]	9.4	[0–38.3]	7.1	[0–24.0]
$Intra_{pre->ver\ (fx4)}$	4.8	[0–22.5]	7.1	[0–40.2]	6.1	[0–22.9]
$Inter_{fx4->fx5}$	4.7	[0–18.3]	7.2	[0–38.1]	6.4	[0–35.8]
$Intra_{Pre->post\ (fx5)}$	4.2	[0–16.4]	6.7	[0–37.2]	4.7	[0–24.6]
$Intra_{pre->ver\ (fx5)}$	3.5	[0–23.1]	5.6	[0–31.5]	4.2	[0–24.0]

and large bowel.

Daily fraction images and daily fraction doses (scaled to 5 fractions) were sequentially deformed, and DVF after each deformation was used to interfractionally accumulate doses ($D0.035cm^3$ and $D5cm^3$) for all 5 patients (Table 2 and Fig. 4). Horizontal dashed line shows the corresponding departmental constraint of 33 Gy for $D0.035cm^3$ and 25 Gy for $D5cm^3$ doses. Two out of five patients had no violations of constraints. One patient exceeded two stomach_duodenum ($D0.035cm^3$ = 36.5 Gy, $D5cm^3$ = 26.1 Gy), and two small bowel ($D0.035cm^3$ = 36.8 Gy, $D5cm^3$ = 26.2 Gy) constraints, while other two patients exceeded two small bowel constraints ($D0.035cm^3$ = 39.4 Gy, $D5cm^3$ = 29.1 Gy) and two stomach_duodenum ($D0.035cm^3$ = 35.8 Gy, $D5cm^3$ = 27.1 Gy) constraints. Treatment was overall well-tolerated in this group of patients, despite several exceeding constraints, with only one patient experiencing Grade1 (mild abdominal pain) acute and late abdominal toxicity (supplementary table 1).

The agreement between the dose-volume parameters calculated using the deformed contour versus the ground-truth contours for the three OARs evaluated using Bland-Altman method showed small mean absolute differences for $D0.035cm^3$, $D2cm^3$ and $D5cm^3$ of 0.3 ± 0.3 Gy, 0.05 ± 0.05 Gy and 0.04 ± 0.06 Gy for stomach_duodenum, 0.5 ± 0.3 Gy, 0.2 ± 0.09 Gy and 0.1 ± 0.07 Gy for small bowel and 0.1 ± 0.08 Gy, 0.02 ± 0.03 Gy and 0.03 ± 0.03 Gy for large bowel, respectively (supplementary Fig. 4).

4. Discussion

In this study, we have quantified the inter and intrafraction deformations and dose accumulation of upper GI organs for LAPC patients undergoing MR-guided ablative SBRT using an in-house developed LDDMM deformable registration method. Our results show that large inter- and intrafraction motion (>10 mm) occurs for upper GI OARs and the LDDMM method produced promising results for the OAR deformations, as evidenced by the high geometric accuracy in the contour overlap measures. Dose accumulation after each treatment fraction using this method showed that DIR accumulated dose metrics exceeded our departmental constraints for three patients while they met for others suggesting the need for dose accumulation tools to further optimize online adaptive planning process.

Out of five patients, three patients exceeded the $D0.035cm^3$ and $D5cm^3$ dose constraint when dose accumulation was applied to manual contours. A clinical consequence of more accurate estimate of dose accumulation to the GI organs is the possibility that target dose coverage can be safely escalated, or OARs can be further spared. Our preliminary results indicate that DIR based dose accumulation may provide the ability to assess the cumulative dose and allow safer delivery of ablative doses to the GTV while sparing near-by OARs. The dose accumulation strategy in this study was based on sequential deformation by registering each fraction image onto the previous fraction's image in a sequential fashion. This can be done offline prior to the next fraction and in future, once streamlined, can be integrated into the online clinical workflow. For adaptive planning, sequential deformation is more intuitive as it gives the total dose delivered to the patient to the point and helps in estimating the residual dose that can potentially be added or subtracted in the next fraction. The process also represents the worst-case estimate as the errors in DIR get accumulated sequentially.

Four of the five patients experienced no acute or late toxicities. The one patient who experienced toxicity had mild (grade 1) acute and late abdominal pain had exceeded two of the duodenal constraints ($D0.035cm^3$, $D5cm^3$). Please see Supplementary table 1 for accumulated dose and toxicity among these five patients. Treatment was overall well-tolerated in this group of patients, despite several exceeding constraints, with only one patient experiencing mild abdominal pain suggesting that (a) location of hotspots in stomach_duodenum may explain the discrepancy between P2 and P4 and (b) our institutional constraints maybe stricter compared to other institutions. Choung et al [29] and Hassanzadeh et al [30] have published the maximum dose constraints to be V40Gy < 0.035 cm^3 and V36Gy < 0.5 cm^3 implying we do need a consensus on GI OAR dose volume constraints for ablative SBRT treatments of locally advanced pancreatic cancer patients. Future analysis of DIR and dose accumulation on a larger patient cohort will further help in understanding the relationship between delivered dose and toxicity.

Our analysis showed that the DSC calculated between LDDMM derived segments and ground truth for all three upper GI organs was between 0.83 and 0.93, which is within the range of AAPM TG-132 recommended DSC values to consider a DIR algorithm sufficiently reliable for clinical deployment [31,32]. Although our results are preliminary due to lack of more reliable measurements such as the target registration error as recommended by the TG-132, these results still show significant improvement over rigid registration and marked improvement over commercial methods. The preliminary results provide the confidence to further evaluate the use of an accurate DIR method for reducing physician contouring time. Current contouring time is around 23 mins with the commercial method as the physician recontours the whole OAR within 2 cm from the PTV because of poor accuracies. In fact, contouring time represents the most time-consuming part of overall online adaptive planning process [19].

In order for a DVF to be reliable, Jacobian integral should have a good agreement with ground-truth volume change (by physician) calculated between the two structures of any fraction. Jacobian integral is calculated from Tensor Based Morphometry [33] that exploits the

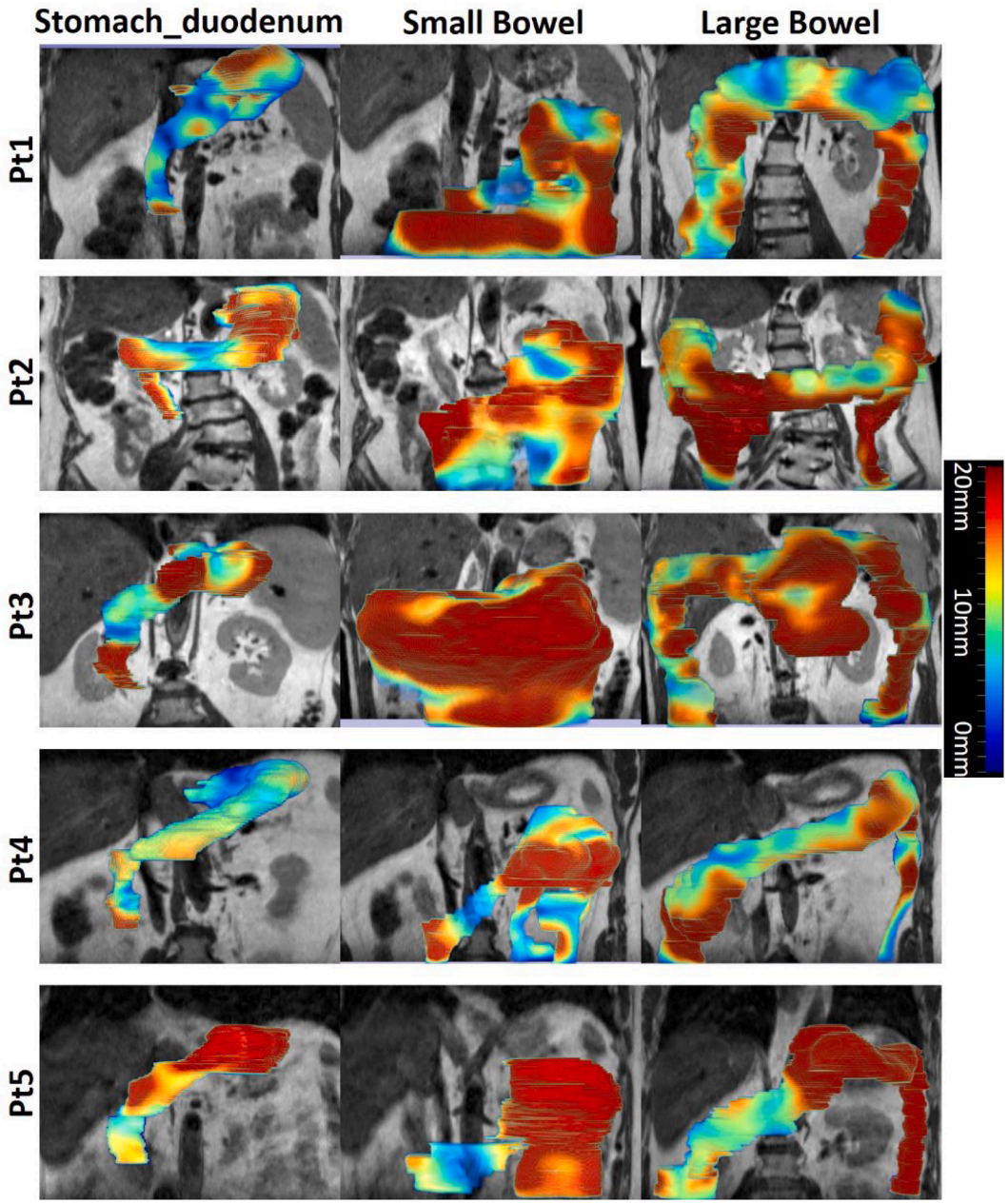

Fig. 3. Regions of largest displacement map of stomach_duodenum, small and large bowels between Fx1 and Fx2 for all five patients.

gradient of a DVF obtained from a DIR to characterize voxel-by-voxel volumetric change of an object [25]. Thus, the local structural changes throughout the volume can be quantified. There are many studies that utilize Jacobian integral to evaluate volumetric changes [22,23,25]. Fuentes et al. [34] and Sarkar et al. [35] used Jacobian map to measure the net volume change of irradiated brain tissue in MRI and liver tumors in CT image, respectively. Both showed that Jacobian map had good agreement with ground-truth segmentation. In our previous work [23], tumor local structural change was quantified in PET and CT images of 61 esophageal cancer patients using Jacobian integral where percentage difference between Jacobian and ground-truth tumor volume changes were small (7.8%). In this study, the correlations between the Jacobian integral and ground-truth volume changes were high for stomach_duodenum, small bowel, and large bowel (supplementary Fig. 1). Main reason could be that in these OARs, the majority of local deformations are morphological elastic and linear shifts. Therefore, DVFs followed straightforward directions and Jacobian could accurately capture their volume changes.

Clinically, during online adaptive planning, the contours are edited within a 2 cm ring around the PTV for faster online planning. This volume includes the relevant dosimetric information including steepest dose gradients [36]. For dose accumulation purpose, contours and doses within the 2 cm volume is not sufficient and may result in incorrect accumulated doses. Hence, OARs were redrawn by an expert physician and deformation and accumulated dose was calculated within the entire patient volume.

Our studies have a few limitations. A total of 75 MRIs from five patients undergoing five MR-guided adaptive treatments were analyzed. Another limitation was the challenge in validating deformable registration results, as is common to all DIR methods [37]. The cost metrics used for optimizing the registration between the MRI scans may need improvement as mean square error measure can be adversely impacted due to differences in MRI signal intensities. However, our results showed clear performance gains compared to rigid registration and investigation

Table 2
Average sequentially accumulated inter and intrafractional D0.035 cm^3 and D5cm^3 doses for stomach_duodenum, small bowell and large bowel.

	Stomach_duodenum		Small Bowel		Large Bowel	
	D0.035cm^3 (Gy)	D5cm^3 (Gy)	D0.035 cm^3 (Gy)	D5cm^3 (Gy)	D0.035cm^3 (Gy)	D5cm^3 (Gy)
$Pre_{(fx1)}$	7.0 ± 1.0	5.1 ± 0.4	7.4 ± 1.4	5.1 ± 0.7	5.5 ± 0.8	4.5 ± 0.6
$Intra\Delta_{Pre\text{-}post\ (fx1)}$	0.1	0.01	0.4	0.07	0.3	0.4
$Intra\Delta_{Pre\text{-}ver\ (fx1)}$	0.2	0.02	0.3	0.07	0.3	0.2
$Inter_{fx1\text{->}fx2}$	13.7 ± 1.4	9.9 ± 0.8	14.2 ± 2.4	10.2 ± 1.8	10.6 ± 2.4	8.6 ± 1.6
$Intra\Delta_{Pre\text{-}post\ (fx2)}$	0.9	0.3	0.4	0.1	0.8	0.7
$Intra\Delta_{Pre\text{-}ver\ (fx2)}$	0.7	0.3	0.5	0.3	1.0	0.6
$Inter_{fx2\text{->}fx3}$	20.4 ± 3.0	15.0 ± 1.6	20.3 ± 3.4	15.2 ± 2.1	14.7 ± 2.5	12.4 ± 1.8
$Intra\Delta_{Pre\text{-}post\ (fx3)}$	0.1	0.3	0.9	0.009	1.1	0.7
$Intra\Delta_{Pre\text{-}ver\ (fx3)}$	0.2	0.2	1.2	0.3	1.1	0.6
$Inter_{fx3\text{->}fx4}$	25.5 ± 3.8	20.7 ± 2.1	28.1 ± 4.7	20.0 ± 2.4	21.9 ± 5.0	16.2 ± 2.3
$Intra\Delta_{Pre\text{-}post\ (fx4)}$	0.9	0.4	0.04	1.2	1.3	0.7
$Intra\Delta_{Pre\text{-}ver\ (fx4)}$	0.4	0.3	0.2	1.0	1.4	0.6
$Inter_{fx4\text{->}fx5}$	31.7 ± 2.7	23.9 ± 1.9	33.2 ± 6.0	25.3 ± 4.8	24.7 ± 5.6	20.1 ± 3.1
$Intra\Delta_{Pre\text{-}post\ (fx5)}$	0.2	0.4	0.2	0.3	1.2	0.7
$Intra\Delta_{Pre\text{-}ver\ (fx5)}$	0.3	0.3	0.2	0.3	1.2	0.6

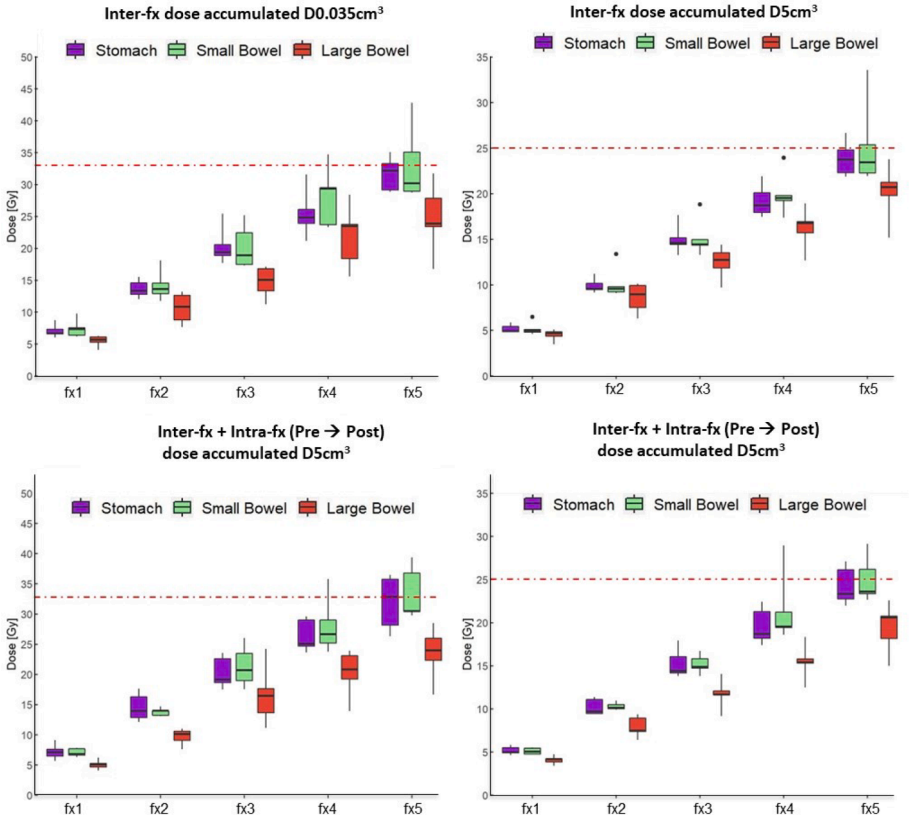

Fig. 4. Box plots showing accumulated dose metrics D0.035cm^3 (left) and D5cm^3 (right) for stomach_duodenum, small bowel and large bowel from interfraction (top row) and intrafraction (bottom row) deformation of all patients for all 5 fractions. Horizontal line represents the departmental constraint of 33 Gy (left) for D0.035cm^3 and 25 Gy (right) for D5cm^3.

of appropriate cost metrics is study for future. Similarly, geometry information that currently relies on clinician generated contours could be impacted by inter-rater variability that can be propagated into the DIR. We plan to address this in the future by using automated segmentation methods using deep learning. In this study, we performed both geometric and dosimetric DIR validations. For the geometric validation, contour statistics such as Hausdorff distance and dice similarity between deformed contours and ground truth physician contours was calculated. For dosimetric evaluation, we took advantage of daily dose map from clinic and calculated the dose-volume parameters difference between the deformed contours and the ground-truth manual contours between the previous and current fractions. Bland Altman plot suggested that the dose metrics derived from deformed contours as well as ground truth physician contours shows minimal dosimetric difference implying good accuracy between DIR propagated contours and ground truth contours. In addition, DVFs used for dose accumulation were validated using Jacobian maps calculated from DIR between the fractions. Finally, the dose accumulation performed in this study was based on physical dose. In future, we will also look into converting physical doses to biological-equivalent dose by applying appropriate biological model for this dose fractionation. Eventually, spatial validation would require use of digital or anthropomorphic phantoms.

In conclusion, LDDMM DIR registration was able to account for large deformations of upper GI organs. Such robust tools for dose

accumulation could allow further personalization of the treatment plans and better correlation to normal tissue toxicity in each fraction with safe dose escalation and reduced treatment toxicities. In future, incorporating prospective dose accumulation to optimize subsequent treatment fractions has potential to achieve more OAR sparing or further escalate target dose by using higher OAR and/or target priority in inverse planning optimization.

5. Ethics approval and consent to participate

The study was conducted under MSKCC IRB approved retrospective protocol.

Declaration of Competing Interest

The authors declare the following financial interests/personal relationships which may be considered as potential competing interests: NT has received honorarium and travel support from Philips and Elekta healthcare. CHC have received travel support from Elekta healthcare.

Acknowledgement

This research was partially supported by the NIH/NCI Cancer Center Support Grant/Core Grant (P30 CA008748).

Appendix A. Supplementary data

Supplementary data to this article can be found online at https://doi.org/10.1016/j.phro.2022.02.007.

References

[1] Siegel RL, Miller KD, Fuchs HE, Jemal A. Cancer Statistics, 2021. CA Cancer J Clin 2021;71:7–33.
[2] Tempero MA, Malafa MP, Al-Hawary M, Behrman SW, Benson AB, Cardin DB, et al. Pancreatic adenocarcinoma, Version 2.2021, NCCN clinical practice guidelines in oncology. J Natl Compr Canc Netw 2021;19:439–57.
[3] Herman JM, Wild AT, Wang H, Tran PT, Chang KJ, Taylor GE, et al. Randomized phase III multi-institutional study of TNFerade biologic with fluorouracil and radiotherapy for locally advanced pancreatic cancer: final results. J Clin Oncol 2013;31:886–94.
[4] Hidalgo M. Pancreatic cancer. N Engl J Med 2010;362:1605–17.
[5] Crane CH. Hypofractionated ablative radiotherapy for locally advanced pancreatic cancer. J Radiat Res 2016;57(Suppl 1):53–7.
[6] Hammel P, Huguet F, van Laethem J-L, Goldstein D, Glimelius B, Artru P, et al. Effect of chemoradiotherapy vs chemotherapy on survival in patients with locally advanced pancreatic cancer controlled after 4 months of gemcitabine with or without erlotinib: the LAP07 randomized clinical trial. JAMA 2016;315:1844–53.
[7] Loehrer PJ, Feng Y, Cardenes H, Wagner L, Brell JM, Cella D, et al. Gemcitabine alone versus gemcitabine plus radiotherapy in patients with locally advanced pancreatic cancer: an Eastern Cooperative Oncology Group trial. J Clin Oncol 2011;29:4105–12.
[8] Reyngold M, Parikh P, Crane CH. Ablative radiation therapy for locally advanced pancreatic cancer: techniques and results. Radiat Oncol 2019;14:95.
[9] Reyngold M, O'Reilly EM, Varghese AM, Fiasconaro M, Zinovoy M, Romesser PB, et al. Association of ablative radiation therapy with survival among patients with inoperable pancreatic cancer. JAMA Oncol 2021;7:735–8.
[10] Boldrini L, Cusumano D, Cellini F, Azario L, Mattiucci GC, Valentini V. Online adaptive magnetic resonance guided radiotherapy for pancreatic cancer: state of the art, pearls and pitfalls. Radiat Oncol 2019;14:71.
[11] Chuong MD, Bryant J, Mittauer KE, Hall M, Kotecha R, Alvarez D, et al. Ablative 5-fraction stereotactic magnetic resonance-guided radiation therapy (MRgRT) with on-table adaptive replanning and elective nodal irradiation for inoperable pancreas cancer. Pract Radiat Oncol 2020.
[12] Rudra S, Jiang N, Rosenberg SA, Olsen JR, Roach MC, Wan L, et al. Using adaptive magnetic resonance image-guided radiation therapy for treatment of inoperable pancreatic cancer. Cancer Med 2019;8:2123–32.
[13] Christiansen RL, Dysager L, Bertelsen AS, Hansen O, Brink C, Bernchou U. Accuracy of automatic deformable structure propagation for high-field MRI guided prostate radiotherapy. Radiat Oncol 2020;15:32.
[14] McDonald BA, Vedam S, Yang J, Wang J, Castillo P, Lee B, et al. Initial feasibility and clinical implementation of daily MR-guided adaptive head and neck cancer radiation therapy on a 1.5T MR-Linac system: prospective R-IDEAL 2a/2b systematic clinical evaluation of technical innovation. Int J Radiat Oncol Biol Phys 2021;109:1606–18.
[15] Liu F, Erickson B, Peng C, Li XA. Characterization and management of interfractional anatomic changes for pancreatic cancer radiotherapy. Int J Radiat Oncol Biol Phys 2012;83:e423–9.
[16] Magallon-Baro A, Loi M, Milder MTW, Granton PV, Zolnay AG, Nuyttens JJ, et al. Modeling daily changes in organ-at-risk anatomy in a cohort of pancreatic cancer patients. Radiother Oncol 2019;134:127–34.
[17] Loi M, Magallon-Baro A, Suker M, van Eijck C, Sharma A, Hoogeman M, et al. Pancreatic cancer treated with SBRT: effect of anatomical interfraction variations on dose to organs at risk. Radiother Oncol 2019;134:67–73.
[18] Han Xu, Hong J, Reyngold M, Crane C, Cuaron J, Hajj C, et al. Deep-learning-based image registration and automatic segmentation of organs-at-risk in cone-beam CT scans from high-dose radiation treatment of pancreatic cancer. Med Phys 2021;48:3084–95.
[19] Tyagi N, Liang J, Burleson S, Subashi E, Godoy Scripes P, Tringale KR, et al. Feasibility of ablative stereotactic body radiation therapy of pancreas cancer patients on a 1.5 Tesla magnetic resonance-linac system using abdominal compression. Phys Imaging Radiat Oncol 2021;19:53–9.
[20] Winkel D, Bol GH, Kroon PS, van Asselen B, Hackett SS, Werensteijn-Honingh AM, et al. Adaptive radiotherapy: The Elekta Unity MR-linac concept. Clin Transl Radiat Oncol 2019;18:54–9.
[21] Tustison NJ, Avants BB. Explicit B-spline regularization in diffeomorphic image registration. Front Neuroinform 2013;7:39.
[22] Alam S, Thor M, Rimner A, Tyagi N, Zhang S-Y, Cheng Kuo Li, et al. Quantification of accumulated dose and associated anatomical changes of esophagus using weekly Magnetic Resonance Imaging acquired during radiotherapy of locally advanced lung cancer. Phys Imaging Radiat Oncol 2020;13:36–43.
[23] Alam RS, Choi W, Liu C, Nadeem S, Tan S, Zhong H, et al. Quantification of local metabolic tumor volume changes by registering blended PET-CT images for prediction of pathologic tumor response. Lect Note Comp Sci 2018;11076:31–41.
[24] Ibanez L, Schroeder W, Ng L, Cates J. The ITK software guide. New York: Insight Toolkit Kitware, Inc.; 2005.
[25] Riyahi S, Choi W, Liu C, Zhong H, Wu A, Mechalakos J, et al. Quantifying local tumor morphological changes with Jacobian map for prediction of pathologic tumor response to chemo-radiotherapy in locally advanced esophageal cancer. Phys Med Biol 2018;63:145020.
[26] Alam SR, Zhang P, Zhang S-Y, Chen I, Rimner A, Tyagi N, et al. Early prediction of acute esophagitis for adaptive radiotherapy. Int J Radiat Oncol Biol Phys 2021;110:883–92.
[27] Chetty IJ, Rosu-Bubulac M. Deformable Registration for dose accumulation. Semin Radiat Oncol 2019;29:198–208.
[28] Bland JM, Altman DG. Agreement between methods of measurement with multiple observations per individual. J Biopharm Stat 2007;17:571–82.
[29] Chuong MD, Bryant J, Mittauer KE, Hall M, Kotecha R, Alvarez D, et al. Ablative 5-fraction stereotactic magnetic resonance-guided radiation therapy with on-table adaptive replanning and elective nodal irradiation for inoperable pancreas cancer. Pract Radiat Oncol 2021;11:134–47.
[30] Hassanzadeh C, Rudra S, Bommireddy A, Hawkins WG, Wang-Gillam A, Fields RC, et al. Ablative Five-fraction stereotactic body radiation therapy for inoperable pancreatic cancer using online MR-guided adaptation. Adv Radiat Oncol 2021;6:100506.
[31] Brock KK, Mutic S, McNutt TR, Li H, Kessler ML. Use of image registration and fusion algorithms and techniques in radiotherapy: Report of the AAPM Radiation Therapy Committee Task Group No. 132. Med Phys. 2017;44:e43-e76.
[32] Paganelli C, Meschini G, Molinelli S, Riboldi Marco, Baroni Guido. Patient-specific validation of deformable image registration in radiation therapy: overview and caveats. Med Phys 2018;45:e908–22.
[33] Ashburner J, Friston KJ. Morphometry. Human brain function. 2 ed: Academic Press; 2004.
[34] Fuentes D, Contreras J, Yu J, He R, Castillo E, Castillo R, et al. Morphometry-based measurements of the structural response to whole-brain radiation. Int J Comput Assist Radiol Surg 2015;10:393–401.
[35] Sarkar S, Narayanan R, Park H, Ma B, Bland PH, Meyer CR. Quantitative growth measurement of lesions in hepatic interval CT exams. Med Imag 2008:6914.
[36] Bohoudi O, Bruynzeel AME, Senan S, Cuijpers JP, Slotman BJ, Lagerwaard FJ, et al. Fast and robust online adaptive planning in stereotactic MR-guided adaptive radiation therapy (SMART) for pancreatic cancer. Radiother Oncol 2017;125:439–44.
[37] Zeng C, Xiong W, Li X, Reyngold M, Gewanter RM, Cuaron JJ, et al. Intrafraction tumor motion during deep inspiration breath hold pancreatic cancer treatment. J Appl Clin Med Phys 2019;20:37–43.